Superfluidity in a gas of strongly interacting fermions

2009 J. Phys.: Condens. Matter 21 164206

(http://iopscience.iop.org/0953-8984/21/16/164206)

J. Phys.: Condens. Matter **21** (2009) 164206 (8pp) doi:10.1088/0953-8984/21/16/164206

Superfluidity in a gas of strongly interacting fermions

W Ketterle, Y Shin, A Schirotzek and C H Schunk

MIT-Harvard Center for Ultracold Atoms, Research Laboratory of Electronics,
Department of Physics, Massachusetts Institute of Technology, Cambridge, MA 02139, USA

E-mail: ketterle@mit.edu

Received 22 January 2009
Published 31 March 2009
Online at stacks.iop.org/JPhysCM/21/164206

Abstract

After an introduction into 100 years of research on superfluidity and the concept of the BCS–BEC crossover, we describe recent experimental studies of a spin-polarized Fermi gas with strong interactions. Tomographically resolving the spatial structure of an inhomogeneous trapped sample, we have mapped out the superfluid phases in the parameter space of temperature, spin polarization, and interaction strength. Phase separation between the superfluid and the normal component occurs at low temperatures, showing spatial discontinuities in the spin polarization. The critical polarization of the normal gas increases with stronger coupling. Beyond a critical interaction strength all minority atoms pair with majority atoms, and the system can be effectively described as a boson–fermion mixture. Pairing correlations have been studied by rf spectroscopy, determining the fermion pair size and the pairing gap energy in a resonantly interacting superfluid.

(Some figures in this article are in colour only in the electronic version)

1. From 1908 to 2008

The field of low-temperature physics has a long tradition. Many people regard the liquefaction of helium in 1908 as the beginning of modern low-temperature physics. At LT25, we celebrated the 100th anniversary of this discovery, and during the conference excursion, many participants of LT25 made a pilgrimage to Leiden, where the original equipment used by Onnes is on display.

This long-standing tradition continues in the research on ultracold bosonic and fermionic atomic gases, and it is interesting to draw a few analogies between current research and what happened 100 years ago. Many cold fermion clouds are cooled by sympathetic cooling with a bosonic atom which is evaporatively cooled into or close to Bose condensation. Popular combinations are ^{6}Li and ^{23}Na (used in our work at MIT), and ^{40}K and ^{87}Rb. It is remarkable that the first fermionic superfluids were also cooled 'sympathetically' by ultracold bosons (liquefied ^{4}He) when Onnes cooled down mercury in 1911, finding that the resistivity of the metal suddenly dropped to nonmeasurable values at $T_C = 4.2$ K, it became 'superconducting'. Tin (at $T_C = 3.8$ K) and lead (at $T_C = 6$ K) showed the same remarkable phenomenon. This was the discovery of superfluidity in an electron gas.

Although superfluidity of bosons was directly observed only in 1938 [1, 2], a precursor was already observed earlier by Onnes when he lowered the temperature of the liquefied ^{4}He below the λ-point at $T_\lambda = 2.2$ K. In his Nobel lecture in 1913, he notes 'that the density of the helium, which at first quickly drops with the temperature, reaches a maximum at 2.2 K approximately, and if one goes down further even drops again. Such an extreme could possibly be connected with the quantum theory' [3]. But instead of studying, what we know now was the first indication of superfluidity of bosons, he first focused on the behavior of metals at low temperatures and observed superconductivity in 1911.

The fact that bosonic superfluidity and fermionic superfluidity were first observed at very similar temperatures, is due to purely technical reasons (because of the available cryogenic methods) and rather obscures the very different physics behind these two phenomena. Bosonic superfluidity occurs at the degeneracy temperature, i.e. the temperature T at which the spacing between particles $n^{-1/3}$ at density n becomes comparable to the thermal de Broglie wavelength $\lambda = \sqrt{\frac{2\pi\hbar^2}{mk_BT}}$, where m is the particle mass. The predicted transition temperature of $T_{BEC} \sim \frac{2\pi\hbar^2}{m}n^{2/3} \approx 3$ K for liquid helium at a typical density of $n = 10^{22}$ cm^{-3} coincides

with the observed lambda point. In contrast, the degeneracy temperature (equal to the Fermi temperature $T_F \equiv E_F/k_B$, where E_F is the Fermi energy) for conduction electrons is higher by the mass ratio $m(^4\mathrm{He})/m_e$, bringing it up to several ten-thousand degrees. Of course, we know now, from the work of Bardeen *et al* [4], that the critical temperature for superfluidity is reduced from the degeneracy temperature to the Debye temperature T_D (since electron–phonon interactions lead to Cooper pairing) times an exponentially small prefactor, $e^{-1/\rho_F|V|}$, with the electron–electron interaction V, attractive for energies smaller than $k_B T_D$ and the density of states at the Fermi energy, $\rho_F = m_e k_F/2\pi^2\hbar^2$. The Debye temperature is typically 100 times smaller than the Fermi energy, and the exponential factor suppresses the transition temperature by another factor of 100, with the result that typical values for T_c/T_F are 10^{-4}.

When the interactions between the electrons are parameterized by an s-wave scattering length a, the transition temperature is given by the expression

$$T_{C,BCS} = \frac{e^\gamma}{\pi}\frac{8}{e^2}E_F e^{-\pi/2k_F|a|} \tag{1}$$

with Euler's constant γ, and $e^\gamma \approx 1.78$. Now, for resonantly interacting fermions (i.e. near a Feshbach resonance), the scattering length a becomes infinite. The above equation is no longer valid, but implies correctly that the transition temperature will approach the Fermi temperature T_F. The value of T_C for $a = \infty$ (i.e. at unitarity) has been calculated analytically [5–8], via renormalization-group methods [9] and via Monte Carlo simulations [10, 11]. The result is $T_C = 0.15$–$0.16T_F$ [8, 11]. It is at the unitarity point that fermionic interactions are at their strongest. Further increase of attractive interactions will lead to the appearance of a bound state and turn fermion pairs into bosons. As a result, the highest transition temperatures for fermionic superfluidity are obtained around unitarity and are on the order of the degeneracy temperature. Finally, almost 100 years after Onnes, it is not just an accidental coincidence anymore that bosonic and fermionic superfluidity occur at similar temperatures! It is in this regime that our experiments are conducted.

2. Ultralow-density condensed matter physics

Many people regard the extremely low nanokelvin temperatures of ultracold atoms as their distinguishing feature. One can take the position that what matters more is their extreme diluteness, at number densities around 10^{13} or 10^{14} cm^{-3}, a million times more dilute than air. With interatomic distances of several 100 nm, the atoms are fairly isolated, and allow the application of all the methods for manipulation and detection developed in atomic physics, including RF spectroscopy, optical detection, preparation in different hyperfine states. Most importantly, since the interactions are short range, these gases are ideal realizations of hard sphere bosons and fermions, idealized by a delta function potential and characterized by the s-wave scattering length. Therefore, their properties are *fully* described by simple Hamiltonians (such as the hard sphere Bose gas, or, when exposed to a periodic potential, by Hubbard models).

This gives cold atoms a new and important link between the materials of the real world with all their richness and complexity, and the simple models used for their description in many-body physics. Often, predictions of models cannot be rigorously tested, because available materials have more complexity (and impurities) than the models, or, with the case of high-T_C superconductors as an example, it is not even clear if the models capture the essential physics of the material. In contrast, using the tools of atomic physics, it is possible to exactly engineer Hamiltonians for ultracold atoms. In this regard, cold atom experiments are quantum simulations of Hamiltonians, but we prefer to say that they realize new forms of matter, which are described by these Hamiltonians.

Of special interest are Hamiltonians which cannot be solved, even numerically. In this case, cold atom experiments may become a tool to verify or falsify whether certain approximation schemes are adequate, i.e. they capture the essential physics either in a qualitative or quantitative way. One example is the fermionic Hubbard model with repulsive interactions [12] suggested as a toy model for high-T_C superconductors, but there is so far no rigorous proof that its ground state is a d-wave superfluid.

The growing list of condensed matter systems which have been realized and studied with cold atoms include the weakly interaction Bose gas [13, 14], the Bose–Hubbard model with the superfluid to Mott insulator transition [15], several regimes of the hard sphere one-dimensional Bose gas (Yang–Yang thermodynamics [16], the Tonks–Girardeau gas [17]), fermions with 'infinite' interaction strength (i.e. resonant interactions in the unitarity limit) [18], the BEC–BCS crossover [18], the Fermi–Hubbard model with the crossover to the Mott insulator [19, 20], and Anderson localization of non-interacting matter waves [21, 22].

3. Realization of the BEC–BCS crossover

When the theory of superconductivity was developed in the 50s, there were controversial discussions about the role of Bose–Einstein condensation. Schafroth, Blatt and Butler speculated that a Bose–Einstein condensate of electron pairs is responsible for superconductivity, but could formalize their ideas only for the case of localized pairs [23]. In contrast, Bardeen, Cooper and Schrieffer pointed out that, for typical conditions, there are around 10^6 electrons in a coherence volume, and therefore the BCS transition is not analogous to Bose–Einstein condensation [4]. We know now that BEC and BCS are the two-limiting cases of the BCS–BEC crossover which smoothly connects the so-called pairing in momentum space (BCS limit) with localized pairs (BEC limit), and the condensation of preformed pairs (the bosons in the BEC limit) with pairing occurring only at the phase transition (BCS).

Soon after the formulation of the BCS theory, Blatt and others showed (see e.g. [24] and references therein) that the BCS wavefunction

$$|\Psi_{BCS}\rangle = \prod_k (u_k + v_k c^\dagger_{k\uparrow} c^\dagger_{-k\downarrow})\,|0\rangle \tag{2}$$

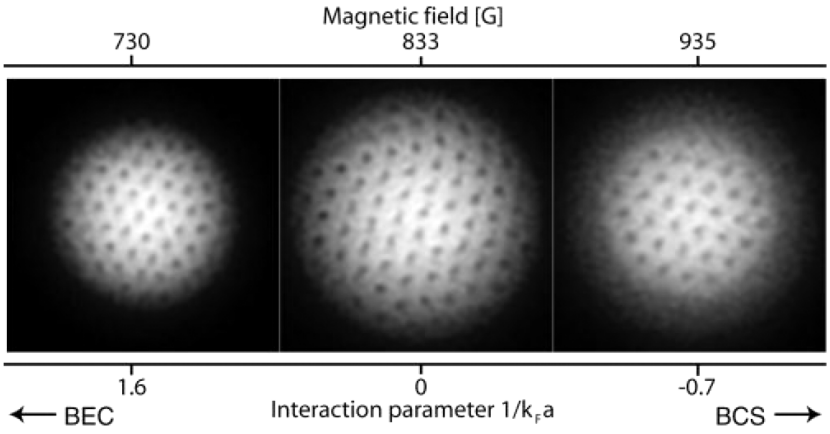

Figure 1. Observation of vortices in a strongly interacting Fermi gas, below, at and above the Feshbach resonance. This establishes superfluidity and phase coherence in fermionic gases. After a vortex lattice was created at 812 G, a field favorable for generating vortices, the field was ramped in 100 ms to 792 G (BEC side), 833 G (resonance) and 853 G (BCS side), where the cloud was held for 50 ms. The field of view of each image is 880 μm × 880 μm. More recent version of figure 3 in [30].

can be expressed as an anti-symmetrized wavefunction of $N/2$ fermion pairs:

$$|\Psi\rangle_N = b^{\dagger N/2}\,|0\rangle\,. \tag{3}$$

In this formulation, the BCS wavefunction mixes up the number of particles (in the spirit of a grand-canonical description), whereas the product of pairs assumes a fixed number of fermions, but both approaches can be formulated for fixed and fluctuating particle numbers.

Here the pair creation operator

$$b^\dagger = \sum_k \varphi_k c^\dagger_{k\uparrow} c^\dagger_{-k\downarrow} \tag{4}$$

is defined using the creation operator $c^\dagger_{k\uparrow}$ for particles with momentum k, the Fourier transform $\varphi(\mathbf{r}_1 - \mathbf{r}_2) = \sum_k \varphi_k \frac{e^{i\mathbf{k}\cdot(\mathbf{r}_1-\mathbf{r}_2)}}{\sqrt{\Omega}}$ of the pair wavefunction $\varphi(\mathbf{r}_1, \mathbf{r}_2)$ and the volume Ω. To write the BCS wavefunction as a 'condensate of pairs' is the essence of the BCS–BEC crossover, since one can now define pair wavefunctions $\varphi(\mathbf{r}_1, \mathbf{r}_2)$ for smaller and smaller pair size and approach the BEC limit of isolated bosons. However, the credit for having predicted the possibility of such a crossover usually goes to Eagles for an early suggestion [25] and to Leggett for a complete presentation of the concept [26].

It is only in the limit of small pairs (i.e. pairs spread out in momentum space), that the pair operators $b^\dagger$ obey bosonic commutation relations. For the commutators, one obtains $[b^\dagger, b^\dagger] = 0$, $[b, b] = 0$ and $[b, b^\dagger] = \sum_k |\varphi_k|^2(1 - n_{k\uparrow} - n_{k\downarrow})$. The third commutator is equal to one only in the limit where the pairs are tightly bound and occupy a wide region in momentum space. In this case, the occupation numbers n_k of any momentum state k are very small and $[b, b^\dagger]_- \approx \sum_k |\varphi_k|^2 = \int \mathrm{d}^3 r_1 \int \mathrm{d}^3 r_2\, |\varphi(\mathbf{r}_1, \mathbf{r}_2)|^2 = 1$.

The realization of the BCS–BEC crossover requires a wide tunability of density [25] or of the attractive interactions between the fermions [26]. After decades of theoretical work, it was only in 2003, that the crossover region was experimentally accessed using ultracold atoms. The tunability of the interactions was implemented using Feshbach resonances. By varying a magnetic field, a (highly vibrationally excited) molecular state is tuned into resonance with two colliding fermions, resulting in a scattering resonance. By tuning across the resonance, the pair size of the fermions could be varied from (somewhat) larger than the interparticle spacing (BCS side) to (somewhat) smaller (BEC side).

In most situations, the onset of superfluidity implies the formation of a pair condensate [27, 18]. The BEC–BCS crossover was first characterized by monitoring the condensate fraction [28, 29], until superfluid flow was directly observed through quantized vortex lattices in rotating clouds [30] (figure 1). The field has been reviewed in the Varenna proceedings [18].

4. Superfluidity with population imbalance

Once a superfluid (or superconducting) system is realized, one characterizes the stability of the superfluid phase by exploring all the possible ways of destroying it, e.g. by raising the temperature, applying a critical magnetic field (which for neutral superfluids would correspond to a critical angular velocity), varying the strength of the interaction, and by imbalancing the population of the spin up and down components. Each way provides a unique insight into the mechanism of pairing. In the BCS picture, pairing occurs preferably at the Fermi surface and therefore becomes energetically less favorable if the two Fermi surfaces do not overlap. Eventually superfluidity will break down when the difference in Fermi energies exceeds the energy gain Δ from pairing. This is the so-called Chandrasekhar–Clogston (CC) limit of superfluidity [31, 32]. Pairing and superfluidity in an imbalanced Fermi mixture has been an intriguing topic for many decades, especially because of the possibility of new exotic ground states such as the Fulde–Ferrell–Larkin–Ovchinnikov (FFLO) state [33, 34] in which either the phase or the density of the superfluid has a spatial periodic modulation.

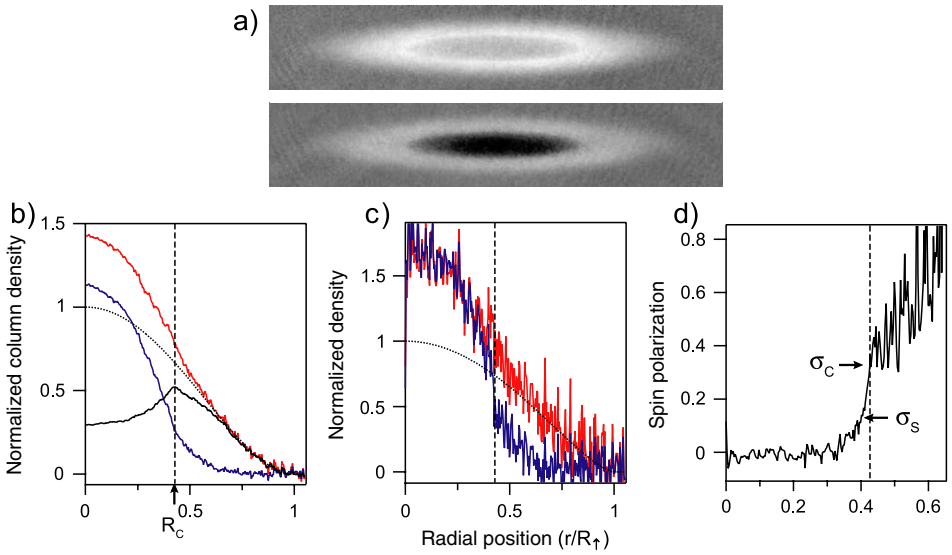

Figure 2. Spatial structure of a trapped Fermi mixture with population imbalance. (a) The *in situ* column density distributions are obtained using a phase-contrast imaging technique [39]. The probe frequencies of the imaging beam are different for the two images so that the first image measures the density difference $n_\uparrow - n_\downarrow$ and the second image measures the weighted density difference $0.76n_\uparrow - 1.43n_\downarrow$. (b) The smooth column density profiles are obtained from the elliptical averaging of the images under the local density approximation (red/upper profile: majority, blue/lower profile: minority, black: difference). (c) The reconstructed three-dimensional density profiles. (d) The spin polarization profile shows a sharp increase, indicating the phase separation between a superfluid core and an outer normal region. The vertical dashed line marks the location of the phase boundary.

Imbalanced Fermi systems can be realized with electron gases by applying a magnetic field. However, the situation in conventional superconductors is more complicated due to spin–orbit coupling, i.e., the field is shielded by the Meissner effect. On the other hand, in atomic Fermi gases one can prepare a mixture with an arbitrary population ratio, since collisional relaxation processes are very slow. A few years ago, using population-imbalanced atomic Fermi gases, a behavior consistent with the CC limit has been observed [35, 36], i.e., a superfluid becomes more robust against imbalance with stronger coupling. The apparent absence of the CC limit in mesoscopic, highly elongated samples [37, 38] is not yet understood and seems to depend on the aspect ratio of the cloud shape.

In the remainder of the paper, we present recent results of the MIT group on the BEC–BCS crossover. One study addresses the phase diagram of a two-component Fermi gas of ^{6}Li atoms with strong interactions. We have identified and/or determined several important critical points including a tricritical point where the superfluid-to-normal phase transition changes from first-order to second-order, critical spin polarizations of the normal phase, and a critical interaction strength where superfluidity can no longer be quenched by population imbalance [39–41]. We also present recently measured rf spectra, where we have determined the fermion pair size and the superfluid gap energy in a resonantly interacting Fermi gas [42, 43].

5. Two-component Fermi mixture in a harmonic potential

In our experiments, we prepared a two-component spin mixture of ^{6}Li atoms, using two states of the three lowest hyperfine states, around a Feshbach resonance. The population imbalance between the two components was controlled by a radio frequency (rf) sweep with an adjustable sweep rate. The atom cloud was confined in a three-dimensional harmonic trap with cylindrical symmetry, thus having an inhomogeneous density distribution. Due to the population imbalance, the chemical potential ratio of the majority (labeled as spin $\uparrow$) and the minority (spin $\downarrow$) components varies spatially over the trapped sample. Under the local density approximation (LDA), each sample represents a line in the phase diagram. Using spatially resolved measurements, we have mapped out the phase diagram of the system. The temperature was controlled by adjusting the trap depth, which determined the final temperature of evaporative cooling.

For typical conditions, the spatial size of our sample was $\sim$150 μm $\times$ 150 μm $\times$ 800 μm with a total atom number of $\sim 10^7$ and a radial (axial) trap frequency of $f_r = 130$ Hz ($f_z = 23$ Hz). Our experiments benefit from the large size of the sample. Using a phase-contrast imaging technique, we obtained the *in situ* column density distributions of the two components $\tilde{n}_{\uparrow,\downarrow}(r)$, and the three-dimensional density profiles $n_{\uparrow,\downarrow}(r)$ were tomographically reconstructed from the averaged column density profiles (figure 2). The imaging resolution of our setup was ~ 2 μm.

At low temperature, the outer part of the sample is occupied by only the majority component, forming a non-interacting Fermi gas. This part fulfils the definition of an ideal thermometer, namely a substance with exactly understood properties in contact with a target sample. We determined the temperature from the in situ majority wing profiles. This *in situ* method provides a clean solution for the long-standing problem of measuring the temperature of a strongly interacting sample.

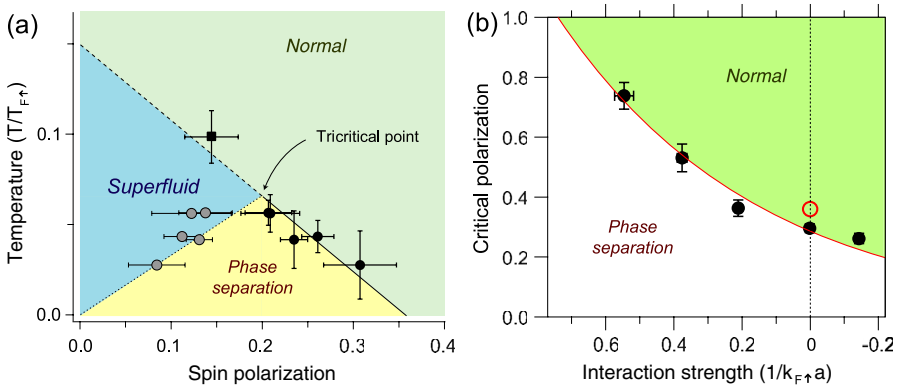

Figure 3. Phase diagram of a two-component Fermi gas with strong interactions. (a) With resonant interactions ($1/k_{F\uparrow}a = 0$). At low temperature, the system shows a first-order superfluid-to-normal phase transition via phase separation, which disappears at a tricritical point where the nature of the phase transition changes from first-order to second-order. (b) The critical polarization σ_c of a partially-polarized normal phase increases with stronger interactions. Above a critical interaction strength ($1/k_{F\uparrow}a \approx 0.7$, $\sigma_c = 1$), even a very small amount of impurity atoms can pair with majority atoms to form a superfluid.

The parameter space of the system can be characterized by three dimensionless quantities: reduced temperature $T/T_{F\uparrow}$, interaction strength $1/k_{F\uparrow}a$ and spin polarization $\sigma = (n_\uparrow - n_\downarrow)/(n_\uparrow + n_\downarrow)$, where $T_{F\uparrow}$ and $k_{F\uparrow}$ are the Fermi temperature and wavenumber of the majority component, respectively, and a is the scattering length of the two components. The standard BCS–BEC crossover physics takes place in the $\sigma = 0$, equal-mixture plane.

6. Phase diagram at unitarity

In the case of fixed particle numbers, it has been suggested that unpaired fermions are spatially separated from a BCS superfluid of equal densities due to the pairing gap energy in the superfluid region [44–46]. At low temperature, we have observed such a phase separation between a superfluid and a normal component in a trapped sample. A spatial discontinuity in the spin polarization clearly distinguishes two regions (figure 2). By correlating a non-zero condensate fraction [35] with the existence of the core region, we verified that the inner core is superfluid [39]. At the phase boundary two critical polarizations σ_s and σ_c are determined for a superfluid and normal phase, respectively. $\sigma_s \neq \sigma_c$ means that there is a thermodynamically unstable window, $\sigma_s < \sigma < \sigma_c$, leading to a first-order superfluid-to-normal phase transition. As the temperature increases, the discontinuity reduces with decreasing σ_c and increasing σ_s, and eventually disappears above a certain temperature. This is a tricritical point where the nature of the phase transition changes from first-order to second-order [47]. Above the tricritical point, the system shows smooth behavior across the superfluid-to-normal phase transition in density profiles and condensate fraction, which is characteristic of a second-order phase transition.

The phase diagram with resonant interactions ($1/k_{F\uparrow}a = 0$) is presented in figure 3(a) [40], characterized by three distinct points: the critical temperature T_{c0} for a balanced mixture, the critical polarization σ_{c0} of a normal phase at zero temperature and the tricritical point (σ_{tc}, T_{tc}). From linear interpolation of the measured critical points, we have estimated $T_{c0}/T_{F\uparrow} \approx 0.15$, $\sigma_{c0} \approx 0.36$ and $(\sigma_{tc}, T_{tc}/T_{F\uparrow}) \approx (0.20, 0.07)$. The quantitative analysis of the *in situ* density profiles at the lowest temperature reveals the equation of state of a polarized Fermi gas [48], showing that the critical chemical potential difference is $2h_c = 2 \times 0.95\mu$, where $\mu = (\mu_\uparrow + \mu_\downarrow)/2$. The pairing gap energy Δ of a superfluid has been measured to be $\Delta \geqslant \mu$ [43], and the observation of $h_c < \Delta$ excludes the existence of a polarized superfluid at zero temperature. A polarized superfluid at finite temperature results from a thermal population of spin-polarized quasiparticles [47].

7. Strongly interacting Bose–Fermi mixture

On the BEC side, two different fermions in free space have a stable bound state, forming a bosonic dimer which undergoes Bose–Einstein condensation at low temperature. Therefore, in the BEC limit a two-component Fermi gas with population imbalance will evolve into a binary mixture of bosonic dimers and unpaired excess fermions. Strong interactions and high degeneracy pressure can affect the structure of the composite boson and eventually quench the superfluid state. This is the reason why we have a partially-polarized normal phase near resonance even at zero temperature. With stronger coupling, the critical polarization σ_c of a partially-polarized normal phase increases, and becomes unity at a critical interaction strength of $1/k_{F\uparrow}a \approx 0.7$ [41]. This means that beyond the critical coupling all minority atoms pair up with majority atoms and form a Bose condensate. This is the regime where a polarized two-component Fermi gas can be effectively described as a Bose–Fermi mixture.

In the limit of a BF mixture [49], we have observed repulsive interactions between the fermion dimers and unpaired fermions. They are parameterized by an effective dimer–fermion scattering length of $a_{bf} = 1.23(3)a$. This value is in reasonable agreement with the exact value $a_{bf} = 1.18a$ which has been predicted over 50 years ago for the three fermion problem [50], but has never been experimentally confirmed. Our finding excludes the mean-field prediction $a_{bf} = (8/3)a$. The boson–boson interactions were found to

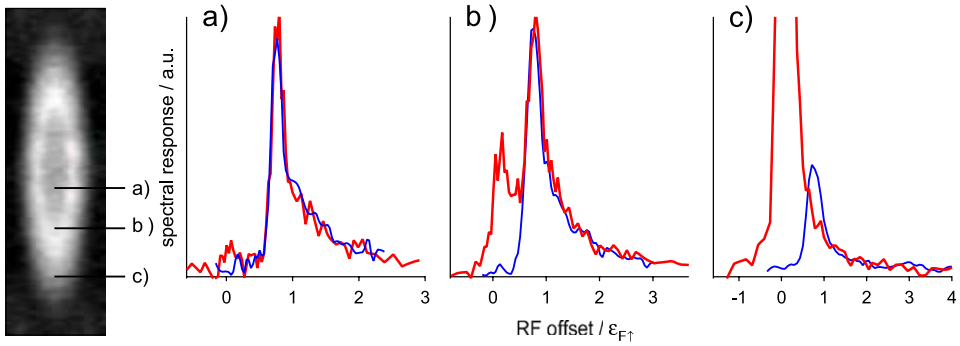

Figure 4. Tomographic RF spectroscopy of strongly interacting Fermi mixtures. A trapped, inhomogeneous sample has various phases in spatially different regions. The spectra of each region (red/upper profile: majority, blue/lower profile: minority) reveals the nature of pairing correlation of the corresponding phase. (a) Balanced superfluid. (b) Polarized superfluid. The additional peak in the majority spectrum is the contribution of the excess fermions, which can be identified as fermionic quasiparticles in a superfluid. From the separation of the two peaks, the pairing gap energy of a resonantly interacting superfluid has been determined [43]. (c) Highly polarized normal gas. The minority peak no longer overlaps with the majority spectrum, indicating the transition to polaronic correlations.

be stronger than the mean-field prediction in agreement with the Lee–Huang–Yang prediction [51]. Including the LHY correction, the effective dimer–dimer scattering length was determined to be $a_{\rm bb} = 0.55(1)a$, which is close to the exact value for weakly bound dimers of $a_{\rm bb} = 0.6a$.

8. Tomographic RF spectroscopy with a new superfluid

RF spectroscopy of a two-component Fermi gas measures a single-particle excitation spectrum by flipping the spin state of an atom to a third spin state. Since a fermion pair can be dissociated via spin flip, RF spectroscopy provides valuable information about the pair such as binding energy and size. In early experiments [52, 53], a spectral shift has been observed in a Fermi gas at low temperature and interpreted as a manifestation of pairing. However, it turned out that the spectral line shape is severely affected by the strong interactions of the third, final spin state and broadened due to the inhomogeneous density distribution of a trapped sample, preventing clear comparison of the experimental results to theory. Recently, we have developed several experimental techniques to overcome these problems. In order to minimize final state effects we have exploited a new spin mixture of states $|1\rangle$ and $|3\rangle$ of ^{6}Li atoms [42] (corresponding to $|F = 1/2, m_{\rm F} = 1/2\rangle$ and $|F = 3/2, m_{\rm F} = -3/2\rangle$ at low field), and using a tomographic technique, we have obtained local RF spectra from an inhomogeneous sample [54].

Figure 4 shows the RF spectra of the various phases in a trapped sample with a population imbalance. For a balanced superfluid, the majority and the minority spectra completely overlap, showing the characteristic behavior of pair dissociation, i.e. a sharp threshold and a slowly decreasing high-energy tail. From the spectral width, we have determined the pair size to be $2.6(2)/k_{\rm F}$ at unitarity, about 20% smaller than the interparticle spacing [42]. These are the smallest pairs so far observed in fermionic superfluids, highlighting the importance of small fermion pairs for superfluidity at high critical temperature [55].

Excess fermions in a low-temperature superfluid constitute quasiparticles populating the minimum of the dispersion curve. The RF spectrum of a superfluid with such quasiparticles shows two peaks, which, in the BCS limit, would be split by the superfluid gap Δ. Therefore, RF spectroscopy of quasiparticles is a direct way to observe the superfluid gap in close analogy with tunneling experiments in superconductors. In a polarized superfluid near the phase boundary, we have obtained a local majority spectrum of a double-peak structure, from which the superfluid gap has been determined to be $\Delta = 0.44(3)E_{\rm F\uparrow}$ at unitarity [43]. In addition, a Hartree term of $-0.43(3)E_{\rm F\uparrow}$ is necessary to explain the observed spectral behavior.

The peak positions of the majority and the minority spectra become different in the partially-polarized normal phase, but still overlap in the high-energy tail. At large spin polarization, the limit of a single minority immersed in a majority Fermi sea is approached, where several theoretical studies suggest a polaron picture, associating the minority with weakly interacting quasiparticles in a normal Fermi liquid [56–58]. We found that these different kinds of pairing correlations are smoothly connected across the superfluid-to-normal phase transition at finite temperature.

9. Summary and discussion

In a series of experiments with population-imbalanced Fermi mixtures near Feshbach resonances, we have established the phase diagram of a two-component Fermi gas with strong interactions. This includes the identification of a tricritical point at which the critical lines for first-order and second-order phase transitions meet, and the verification of a zero-temperature quantum phase transition from a balanced superfluid to a partially-polarized normal gas at unitarity. The observed critical points such as the critical polarization of a normal phase and the critical interaction strength of a composite boson in a Fermi sea provide quantitative tests for theoretical treatments of strongly interacting fermions.

Our work can be summarized with the phase diagram of the system in a 3D parameter space (versus temperature, spin

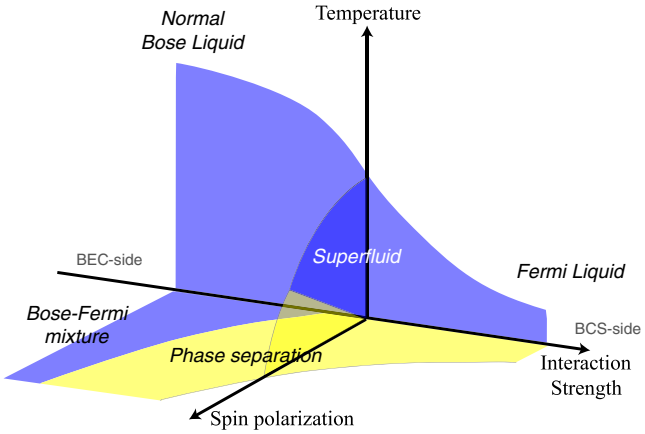

Figure 5. Various phases of a two-component Fermi gas. The structure of the phase diagram is illustrated in the parameter space of temperature, interaction strength and spin polarization.

polarization and interaction strength) shown in figure 5. For a complete understanding, this macroscopic characterization of the different phases should be complemented by an investigation of their microscopic properties. At low temperature, one can interpret the observed polarized superfluid as a result of a thermal population of spin-polarized quasiparticles. However, the behavior at higher temperature or/and in a stronger coupling regime is not yet completely understood and could include a gapless region ($h > \Delta$). The nature of a partially-polarized normal phase near the resonance is also an interesting subject. Measurement of the binding energy and the effective mass of a minority atom might test the polaron picture and establish the polaron-to-molecule transition near a critical interaction strength. Another open question is whether the Fermi liquid description is still valid for high minority concentrations, where Pauli blocking in the minority Fermi sea might play an important role. Furthermore, it has been speculated that exotic pairing states might exist in the partially-polarized phase [59]. So far, predicted exotic superfluid states such as the breached-pair state in a stronger coupling regime and the FFLO state in a weaker coupling regime have not been observed, but they may be hidden in thin layers near the superfluid–normal boundary. This discussion underlines that the population-imbalanced Fermi system is the richest system realized thus far with ultracold gases and therefore nicely illustrates the novel approach to engineer interesting many-body systems using the tools and methods of atomic physics.

Acknowledgments

This work was supported by NSF, ONR, MURI and ARO Award W911NF-07-1-0493 (DARPA OLE Program).

References

[1] Kapitza P 1938 *Nature* **141** 74
[2] Allen J F and Misener A D 1938 *Nature* **141** 75
[3] Onnes K 1967 *Nobel Lectures, Physics 1901–1921* (Amsterdam: Elsevier)
[4] Bardeen J, Cooper L N and Schrieffer J R 1957 *Phys. Rev.* **108** 1175
[5] Nozières P and Schmitt-Rink S 1985 *J. Low Temp. Phys.* **59** 195
[6] de Melo C A R S, Randeria M and Engelbrecht J R 1993 *Phys. Rev. Lett.* **71** 3202
[7] Hu H, Liu X J and Drummond P D 2006 *Phys. Rev.* A **73** 023617
[8] Haussmann R, Rantner W, Cerrito S and Zwerger W 2007 *Phys. Rev.* A **75** 023610
[9] Nishida Y and Son D T 2006 *Phys. Rev. Lett.* **97** 050403
[10] Bulgac A, Drut J E and Magierski P 2006 *Phys. Rev. Lett.* **96** 090404
[11] Burovski E, Prokofev N, Svistunov B and Troyer M 2006 *Phys. Rev. Lett.* **96** 160402
[12] Scalapino D J 1995 *Phys. Rep.* **250** 329
[13] Cornell E A and Wieman C E 2002 *Rev. Mod. Phys.* **74** 875
[14] Ketterle W 2002 *Rev. Mod. Phys.* **74** 1131
[15] Greiner M, Mandel O, Esslinger T, Hansch T W and Bloch I 2002 *Nature* **415** 39
[16] van Amerongen A H, van Es J J, Wicke P, Kheruntsyan K V and van Druten N J 2008 *Phys. Rev. Lett.* **100** 090402
[17] Kinoshita T, Wenger T and Weiss D S 2004 *Science* **305** 1125
[18] Incuscio M, Ketterle W and Salomon C (ed) 2007 Ultra-cold fermi gases *Proc. Int. School of Physics 'Enrico Fermi' Course CLXIV* (Amsterdam: IOS Press)
[19] Jordens R, Strohmaier N, Gunter K, Moritz H and Esslinger T 2008 *Nature* **455** 204
[20] Schneider U, Hackermuller L, Will S, Best T, Bloch I, Costi T A, Helmes R W, Rasch D and Rosch A 2008 *Science* **322** 1520
[21] Billy J, Josse V, Zuo Z, Bernard A, Hambrecht B, Lugan P, Clement D, Sanchez-Palencia L, Bouyer P and Aspect A 2008 *Nature* **453** 891
[22] Roati G, D'Errico C, Fallani L, Fattori M, Fort C, Zaccanti M, Modugno G, Modugno M and Inguscio M 2008 *Nature* **453** 895
[23] Schafroth M R, Butler S T and Blatt J M 1957 *Helv. Phys. Acta* **30** 93
[24] Baranger M 1963 *Phys. Rev.* **130** 1244
[25] Eagles D M 1969 *Phys. Rev.* **186** 456
[26] Leggett A J 1980 *Modern Trends in the Theory of Condensed Matter* (Berlin: Springer) pp 13–27
[27] Bloch I, Dalibard J and Zwerger W 2008 *Rev. Mod. Phys.* **80** 885
[28] Regal C A, Greiner M and Jin D S 2004 *Phys. Rev. Lett.* **92** 040403
[29] Zwierlein M W, Stan C A, Schunck C H, Raupach S M F, Kerman A J and Ketterle W 2004 *Phys. Rev. Lett.* **92** 120403
[30] Zwierlein M W, Abo-Shaeer J R, Schirotzek A, Schunck C H and Ketterle W 2005 *Nature* **435** 1047
[31] Chandrasekhar B S 1962 *Appl. Phys. Lett.* **1** 7
[32] Clogston A M 1962 *Phys. Rev. Lett.* **9** 266
[33] Fulde P and Ferrell R A 1964 *Phys. Rev.* **135** A550
[34] Larkin A I and Ovchinnikov Y N 1965 *Sov. Phys.—JETP* **20** 762
[35] Zwierlein M W, Schirotzek A, Schunck C H and Ketterle W 2006 *Science* **311** 492
[36] Zwierlein M W, Schunck C H, Schirotzek A and Ketterle W 2006 *Nature* **442** 54
[37] Partridge G B, Li W, Karmar R I, Liao Y and Hulet R G 2006 *Science* **311** 503
[38] Partridge G B, Li W, Karmar R I, Liao Y and Hulet R G 2006 *Phys. Rev. Lett.* **97** 190407
[39] Shin Y, Zwierlein M W, Schunck C H, Schirotzek A and Ketterle W 2006 *Phys. Rev. Lett.* **97** 030401
[40] Shin Y, Schunck C H, Schirotzek A and Ketterle W 2008 *Nature* **451** 689
[41] Shin Y, Schunck C H, Schirotzek A and Ketterle W 2008 *Phys. Rev. Lett.* **101** 070404

[42] Schunck C H, Shin Y, Schirotzek A and Ketterle W 2008 *Nature* **454** 739
[43] Schirotzek A, Shin Y, Schunck C H and Ketterle W 2008 *Phys. Rev. Lett.* **101** 140403
[44] Bedaque P F, Caldas H and Rupak G 2003 *Phys. Rev. Lett.* **91** 247002
[45] Carlson J and Reddy S 2005 *Phys. Rev. Lett.* **95** 060401
[46] Sheehy D E and Radzihovsky L 2006 *Phys. Rev. Lett.* **96** 060401
[47] Parish M M, Marchetti F M, Lamacraft A and Simons B D 2007 *Nat. Phys.* **3** 124
[48] Shin Y 2008 *Phys. Rev.* A **77** 041603(R)
[49] Pieri P and Strinati G C 2006 *Phys. Rev. Lett.* **96** 150404
[50] Skorniakov G V and Ter-Martirosian K A 1957 *Sov. Phys.—JETP* **4** 648
[51] Lee T D, Huang K and Yang C N 1957 *Phys. Rev.* **106** 1135
[52] Chin C, Bartenstein M, Altmeyer A, Riedl S, Jochim S, Denschlag J H and Grimm R 2004 *Science* **305** 1128
[53] Schunck C H, Shin Y, Schirotzek A, Zwierlein M W and Ketterle W 2007 *Science* **316** 867
[54] Shin Y, Schunck C H, Schirotzek A and Ketterle W 2007 *Phys. Rev. Lett.* **99** 090403
[55] Pistolesi F and Strinati G C 1994 *Phys. Rev.* B **49** 6356
[56] Lobo C, Recati A, Giorgini S and Stringari S 2006 *Phys. Rev. Lett.* **97** 200403
[57] Combescot R, Recati A, Lobo C and Chevy F 2007 *Phys. Rev. Lett.* **98** 180402
[58] Prokof'ev N and Svistunov B 2008 *Phys. Rev.* B **77** 020408(R)
[59] Bulgac A, Forbes M M and Schwenk A 2006 *Phys. Rev. Lett.* **97** 020402